Supercontinuum generated in all-normal dispersion photonic crystal fibers with picosecond pump pulses*

Li Pan(李 磐), Shi Lei(时 雷), and Mao Qing-He(毛庆和)†

Anhui Provincial Key Laboratory of Photonics Devices and Materials, Anhui Institute of Optics and Fine Mechanics, Chinese Academy of Sciences, Hefei 230031, *China*

(Received 22 January 2013; revised manuscript received 21 March 2013)

The supercontinuum (SC) generation in all-normal dispersion (ANDi) photonic-crystal fiber (PCF) pumped by high power picosecond pulses are investigated in this paper. Our results show that an octave SC may be achieved by pumping the ANDi PCF with picosecond pump pulses. However, the PCF length required may have to be lengthened to several tens of centimeters, which is much longer than that with femtosecond pump pulses. The relatively long PCF gives rise to much higher Raman gain and stronger Raman frequency shift compared to those with femtosecond pump pulses, which in turn not only cause a distorted temporal waveform and an un-flattened spectrum, but also severely degrade the coherence of the generated SC.

Keywords: supercontinuum generation, photonic crystal fibers, optical wave breaking

PACS: 42.55.Wd, 42.65.Tg, 42.81.–i **DOI:** 10.1088/1674-1056/22/7/074204

1. Introduction

High-brightness supercontinuum (SC) light sources have many important applications in frequency metrology,[1] coherence tomography,[2] nonlinear microscopy,[3,4] and ultrashort pulse generation.[5] Various nonlinear waveguides have been proposed for the SC generation with different pump pulses.[6–8] With the enhanced nonlinearity and tailorable dispersion profiles, photonic crystal fibers (PCFs) have brought a revolutionary progress to the SC generation in the past decade.[9,10] To date, more than one octave SC can be easily generated with a piece of highly nonlinear PCF pumped by femtosecond or picosecond pulses near the zero-dispersion wavelength (ZDW) in the anomalous group velocity dispersion (GVD) regime of the PCF.[11–13] Generally speaking, the spectral broadenings in an anomalous GVD PCF for femtosecond and picosecond pump pulses are dominated by the soliton effect which breaks up the pump pulse into a series of fundamental solitons due to the soliton fission, and the modulation instability (MI) which transfers the pump pulse energy to the two sidebands continuously to form modulation profiles in the time domain that finally also evolve into fundamental solitons,[14] respectively. These fundamental solitons are then individually Raman-shifted to longer wavelengths and in turn gradually separate from each other to form many sub-pulses in the temporal domain due to the fiber dispersion, resulting in a very complex temporal profile for the SC.[15] The previous research results have shown that the generated SC in the anomalous GVD PCF is very sensitive to the pump pulse fluctuation and laser shot noise, giving rise to great differences in the spectral structure from pulse to pulse and the degradation of coherence across the SC spectral bandwidth. Especially, when the soliton order or the duration of the injected pump pulse is larger than 40 or 100 fs, the generated SC will then possess a very low coherence.[16,17] This indicates that it may be very difficult to generate SC with both high coherence and high power spectral density using pump pulses near the ZDW in the anomalous GVD regime of the PCF.

Recent theoretical and experimental research results have shown that SCs with a high coherence, a flattened spectrum, and a single time-domain waveform can be generated by pumping all-normal dispersion (ANDi) PCF with high peak power femtosecond pulses because there is no soliton effect.[18–20] In fact, the power spectral density is also a very important specification parameter for the SC in many practical applications. Obviously, the power spectral density may be enhanced by increasing the single pulse energy of the pump pulse for a given repetition rate. However, as is well known, it is much more difficult to obtain large single pulse energy for the femtosecond pulse than that for the picosecond pulse because of the limitation of various fiber nonlinearities in pulse amplification and compression processes. Unfortunately, to our best knowledge, almost all the reports on the SC generation in ANDi PCF so far are based on femtosecond or subpicosecond pump pulses. For instance, the longest pump pulse used for the simulations of the SC generation in the ANDi PCF is about 300 fs, where the generated SC in the ANDi PCF may still possess excellent temporal waveform, flattened spectrum, and high coherence.[18] Therefore, it is necessary to investi-

*Project supported by the National High Technology Research and Development Program of China (Grant No. 2011AA030203), the National Natural Science Foundation of China (Grant No. 61250017), and the Key Research Program of the Chinese Academy Sciences (Grant No. KJZD-EW-W02).

†Corresponding author. E-mail: mqinghe@aiofm.ac.cn

© 2013 Chinese Physical Society and IOP Publishing Ltd

gate the SC generation in the ANDi PCF and the coherence of the generated SC when picosecond pulses are use as the pump.

In this paper, the SC generation dynamics in the ANDi PCF pumped by picosecond pulses are numerically investigated with the scalar generalized nonlinear Schrödinger equation (GNLSE). Our simulation results show that an octave SC may be equally achieved by pumping the ANDi PCF with picosecond pulses. However, the PCF length required for the octave SC generation with picosecond pump pulses may have to be lengthened to several tens of centimeters, which is much longer than that with femtosecond pump pulses. Since a relatively long PCF is used, the Raman gain is much higher and the Raman frequency shift is much stronger in the SC generation process compared to those for femtosecond pump pulses. The high Raman gain and strong Raman frequency shift in turn not only cause a distorted temporal waveform and an un-flattened spectrum with sub-structures, but also severely degrade the coherence of the generated SC.

2. Theoretical model

A picosecond pump pulse propagating in the ANDi PCF may be governed by the following scalar GNLSE:[14]

$$\frac{\partial A(z,t)}{\partial z}+\frac{\alpha}{2}A(z,t)-\sum_{k\geq 2}\frac{\mathrm{i}^{k+1}}{k!}\beta_k\frac{\partial^k A(z,t)}{\partial t^k}$$
$$=\mathrm{i}\gamma\left(1+\mathrm{i}\tau_{\mathrm{shock}}\frac{\partial}{\partial t}\right)$$
$$\times\left\{A(z,t)\left[\int_{-\infty}^{+\infty}R(t')\times|A(z,t-t')|^2\,\mathrm{d}t'+\mathrm{i}\Gamma_{\mathrm{R}}(z,t)\right]\right\}, \quad (1)$$

where $A(z,t)$ is the complex field envelope in a co-moving frame; β_k stand for the dispersion coefficients of the PCF, which are associated with the Taylor expansion of the propagation constant around the center frequency ω_0; γ is the nonlinear coefficient of the PCF; and α is the fiber loss, which is neglected here since only a short PCF is used. The time derivative in the nonlinear operator includes the effects of self-steepening and optical shock formation, which are characterized on the time scale of $\tau_{\mathrm{shock}}=1/\omega_0$. The response function $R(t')=(1-f_{\mathrm{R}})\delta(t)+f_{\mathrm{R}}h_{\mathrm{R}}(t)$ contains both instantaneous and delayed Raman contributions, with $f_{\mathrm{R}}=0.18$ standing for the fractional delayed Raman contribution and $h_{\mathrm{R}}(t)$ for the Raman response function of the PCF with the analytical expression given in Ref. [21]. The $\Gamma_{\mathrm{R}}(z,t)$ describes the spontaneous Raman scattering and has the frequency domain correlation[14]

$$\langle\Gamma_{\mathrm{R}}(\Omega,z)\Gamma_{\mathrm{R}}^{*}(\Omega',z')\rangle$$
$$=\frac{2f_{\mathrm{R}}\hbar\omega_0}{\gamma}|\mathrm{Im}[h(\Omega)]|[n_{\mathrm{th}}(|\Omega|)+U(-\Omega)]$$
$$\times\delta(z-z')\delta(\Omega-\Omega'), \quad (2)$$

with $n_{\mathrm{th}}(\Omega)=[\exp(\hbar\Omega/k_{\mathrm{B}}T)-1]^{-1}$, $R(t')=(1-f_{\mathrm{R}})\delta(t)+f_{\mathrm{R}}h_{\mathrm{R}}(t)$ and $U(\Omega)$ respectively being the thermal Bose distribution and the Heaviside step function, and $\Omega=\omega-\omega_0$.

For estimating the coherence of the generated SC, the quantum-limited noise of the input pump is taken into account by phenomenologically adding one photon per mode with a random phase on each spectral discretization bin at the input end of the PCF. The noise sensitivity of the generated SC is then characterized by calculating the modulus of the complex degree of the first-order coherence at each wavelength λ [14]

$$|g_{12}^{1}(\lambda,t_1-t_2)|=\left|\frac{\langle E_1(\lambda,t_1)E_2(\lambda,t_2)\rangle}{\sqrt{\langle|E_1(\lambda,t_1)|^2\rangle\langle E_2(\lambda,t_2)|^2\rangle}}\right|, \quad (3)$$

where the angular bracket indicates an ensemble average over independently generated pairs of SC spectra obtained from 100 simulations, and t is the time measured at the scale of the temporal resolution of the spectrometer used. The wavelength dependence of the coherence for the generated SC can then be calculated by setting $t_1-t_2=0$ in Eq. (3). The coherence at each wavelength may be estimated by the value of $|g_{12}^{1}(\lambda)|$, which is located in the interval [0, 1], with $|g_{12}^{1}(\lambda)|=1$ representing perfect coherence.

Many simulation methods may be used for solving the scalar GNLSE (1).[21–24] In our simulations, Eq. (1) is solved with the Runge–Kutta in the interaction picture (RK4IP) method in frequency domain for the SC generation, and the calculation precision is ensured by controlling the relative error of the conservation quantity of the optical photon number between input and output ends to be less than 5%.[21,23] The dispersion profile of the PCF used in the simulations is shown in Fig. 1, which is similar to that of PCF NL-1050-NEG-1 produced by NKT Photonics.[25] All input pulses are of the chirp-free Gaussian shape, i.e., $A(0,t)=\sqrt{P_0}\exp(-t^2/2t_0^2)$, with t_0 being the half-width at 1/e intensity, which satisfies $t_{\mathrm{FWHM}}\approx 1.665t_0$. Table 1 lists the center wavelength of the input pulse, the dispersion parameters which are fitted according to the dispersion curve in Fig. 1, and the nonlinear coefficient.

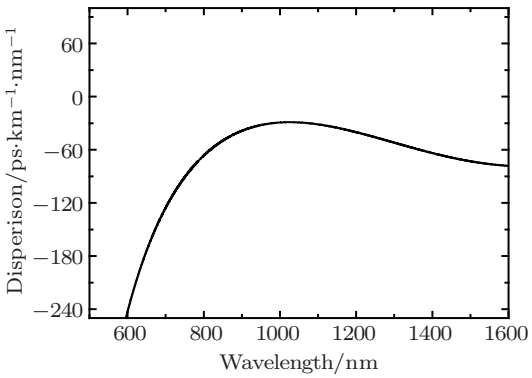


Fig. 1. Dispersion curve of the PCF.

Table 1. Parameters used in simulations.

β_2	2.2590×10^{-2} ps^2·m^{-1}	β_3	-4.0444×10^{-5} ps^3·m^{-1}
β_4	2.5464×10^{-7} ps^4·m^{-1}	β_5	-1.0273×10^{-9} ps^5·m^{-1}
β_6	2.8644×10^{-12} ps^6·m^{-1}	β_7	1.3131×10^{-14} ps^7·m^{-1}
β_8	-1.9999×10^{-16} ps^8·m^{-1}	β_9	1.0332×10^{-18} ps^9·m^{-1}
β_{10}	-2.6889×10^{-21} ps^{10}·m^{-1}	β_{11}	2.9639×10^{-24} ps^{11}·m^{-1}
γ	0.037 W^{-1}·m^{-1}	λ_0	1060 nm

3. Results and discussion

We first numerically simulate the SC generation process in the ANDi PCF with picosecond pump pulses. As the pulse energy of a picosecond pulsed mode-locked fiber laser may reach hundreds nanojoules[28,29] and the high energy picosecond pulses have already been applied for the SC generation in the conventional PCF,[12] in our simulations the input pump picosecond pulses with the peak power of 60–90 kW are chosen for investigating the SC generation dynamics. Figure 2 shows spectral and temporal evolutions for input picosecond pulses with different peak powers and durations. For the convenience of comparison, the evolutions of 50 fs and 300 fs pump pulses are also given in the figure. As shown, an octave SC can be generated when the PCF is pumped with picosecond pulses, while in contrast, the power spectral density of the generated SC pumped with picosecond pulses is much higher than that with femtosecond pulses. Pumped with 50 fs and 300 fs pulses, octave SCs from 700 nm to 1500 nm can respectively be obtained by using only about 0.8 cm and 6 cm PCFs. And the generated SCs both possess an excellent temporal waveform and a flattened spectrum as those reported in Ref. [18]. When the PCF is pumped with picosecond pulses, the PCF lengths required for the octave SC generation are much longer, and the spectral and temporal broadening processes of the pump pulses in the PCF are very complicated. In the first section of the PCF, the spectra of the input picosecond pulses are approximately broadened linearly while their durations are increased very slightly. For the input pulses with the peak powers and durations of 60 kW and 2 ps, 90 kW and 2 ps, and 90 kW and 4 ps, the spectra are broadened suddenly to nearly an octave with two asymmetric sidebands at the propagation distances of about 19 cm, 14.5 cm, and 30 cm, respectively, as shown in Fig. 2. After that, as the propagation distance increases, the durations of all the pump pulses are approximately increased linearly while their spectral bandwidths are basically unchanged except that the two asymmetric sidebands are gradually merged into the pump pulse spectrum. However, after having propagated for about 60 cm, 48 cm, and 55 cm, respectively, some sub-structures unexpectedly appear near the spectral positions where the short wavelength sidebands merge into the pump pulse spectra.

In order to understand the SC generation dynamics in the PCF with picosecond pump pulses, in particular, the unexpected sub-structures in the broadened SCs, the time-frequency distribution properties of the pulses at different propagation distances in the PCF are further analyzed. Figure 3 shows such spectrograms for the same input pump pulse shown in Figs. 2(b) and 2(g). When the pulse propagates 10 cm along the PCF, as shown in Fig. 3(a), the spectrogram exhibits the self-phase modulation (SPM) characteristic, i.e., S-shaped feature with a red shift and a blue shift on the leading and the trailing edges, respectively.[19] The broadened frequency spectrum has an overlapped oscillatory structure due to

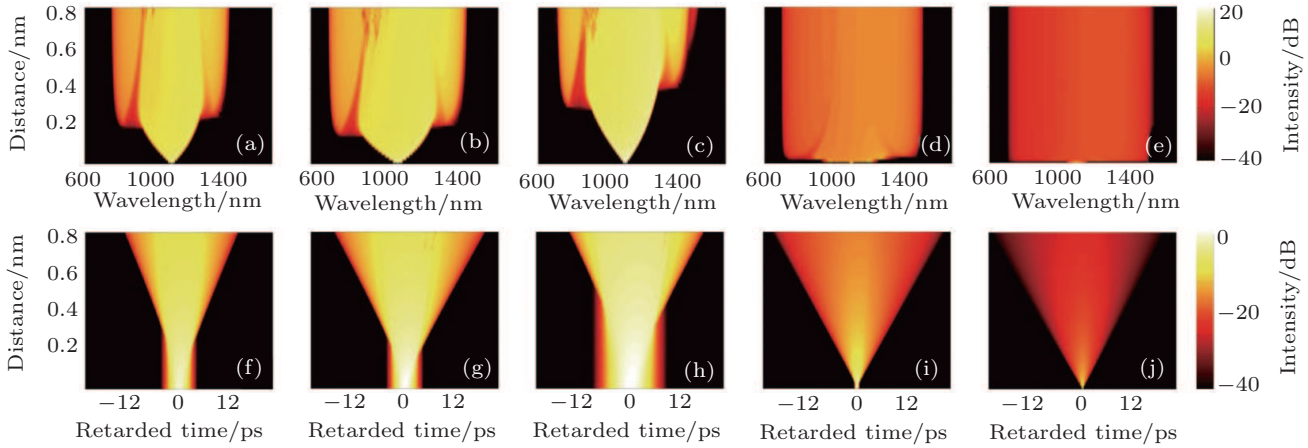


Fig. 2. (color online) Spectral and temporal evolutions along the PCF for pump pulses with different peak powers and durations: (a) and (f): 60 kW and 2 ps; (b) and (g): 90 kW and 2 ps; (c) and (h): 90 kW and 4 ps; (d) and (i): 90 kW and 300 fs; and (e) and (j): 90 kW and 50 fs. The intensities in frequency and time domains are normalized by the maximum spectral density in panel (e) and the maximum peak power in panel (j), respectively.

the SPM, and the temporal duration is almost unchanged. As the red- and blue-shift chirps on the leading and trailing edges are accumulated when the pulse continues to propagate along the PCF, the chirp of the pulse becomes nonmonotonic with the combined effects of SPM and GVD.[26] In the PCF, the lower instantaneous frequency components near the leading edge travel faster and overtake the higher instantaneous frequency components in the forward tail of the pulse, while the opposite occurs for the high instantaneous frequency components near the trailing edge, and thus, the optical wave breaking (OWB) sets on, making the temporal overlap of two pulse components with different instantaneous frequencies generate interference beating in the pulse temporal profile, which in turn creates new frequencies though degenerate four-wave mixing (FWM) in the frequency domain.[19,27] At the propagation distance of 20 cm, as shown in Fig. 3(b), the two new sidebands caused by OWB and FWM can be clearly seen. Note that the two sidebands are asymmetric, this is because the self-steepening before FWM and OWB has already led to an asymmetric SPM-induced spectral broadening.[15] The simulated propagation distance for OWB and FWM is about 14.5 cm (see Fig. 2(b)), which is in agreement with the calculation result of 14.66 cm according to Refs. [26] and [27], and is obviously much longer than that of the femtosecond pulses (see Figs. 2(d) and 2(e)). The reason is that the input picosecond pulse has a narrower spectrum, thus its spectrum has to be broadened with the help of SPM and GVD in a relatively long PCF to make OWB and FWM take place. At the propagation distance of 40 cm, the spectrogram in Fig. 3(c) becomes a near oblique straight line, indicating that the two sidebands created by OWB have basically merged into the whole spectral profile. This implies that the effective degenerate FWM may have almost finished. Thus, the temporally broadening due to GVD is strengthened because of the greatly broadened spectrum. At 60 cm, the slope of the oblique straight line as seen from the spectrogram in Fig. 3(d) becomes smaller compared to that in Fig. 3(c) because of the GVD, i.e., the spectral bandwidth is almost unchanged while the temporal broadening continues as it is before. However, some new frequency disarrangements apear, displayed in Fig. 3(d) as two separate vertical lines overlap on both sides of the oblique straight line right at the place where the short wavelength sideband generated by OWB is merged into the pulse spectrum. Moreover, these new created frequency components become stronger when the propagation distance is 80 cm (Fig. 3(e)), where the lines grow into a wider and vertical space, and finally form a peculiar range with an even higher density in the middle of the line at 100 cm (Fig. 3(f)).

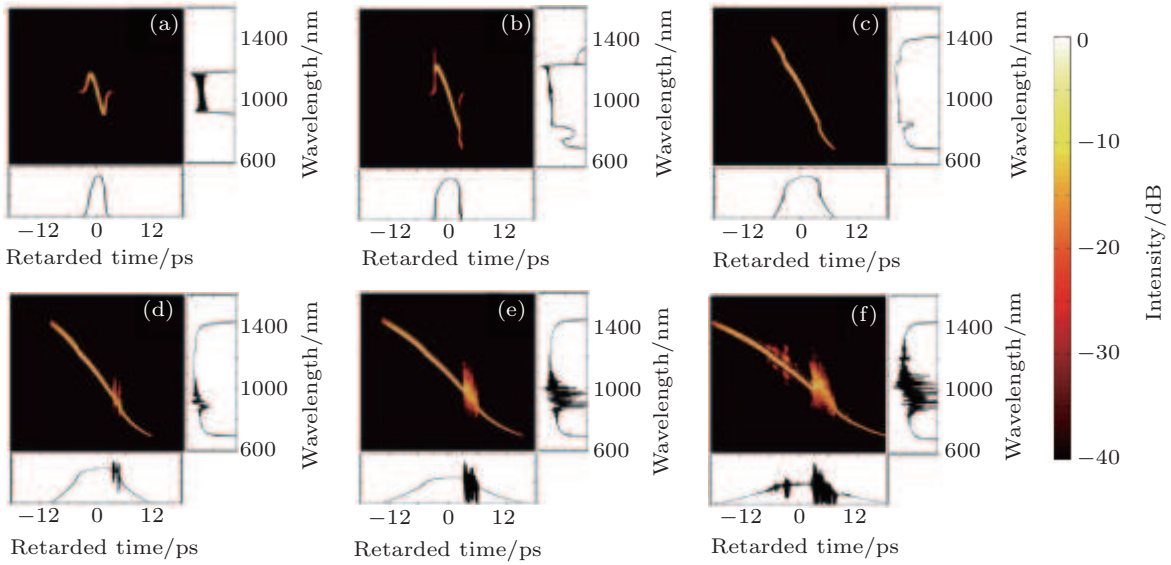


Fig. 3. (color online) Time-frequency distributions for input pump pulse of 90 kW and 2 ps at different propagation distances ((a) 10 cm, (b) 20 cm, (c) 40 cm, (d) 60 cm, (e) 80 cm, (f) 100 cm). All the figures are normalized by the corresponding maximum values.

In general, the new created frequency components shown in Figs. 3(d)–3(f) may be caused by MI, FWM, or stimulated Raman scattering (SRS). However, by calculating the gain spectrum of MI with $K = \mathrm{Im}\sqrt{Q(Q+2/L_{\mathrm{NL}})}$, where L_{NL} is the nonlinear length, $Q = \sum \beta_k \Omega^k / k!$, and k is a positive even integer,[9] we find that the gain band of MI is located at more than 200 THz away from the center frequency, which is not the case shown in Figs. 3(d)–3(f). In addition, since the newly created frequency components overlapped on the upper-side cover wider frequency range than those on the downside of the oblique straight line, as shown in Figs. 3(d)–3(f), they cannot be caused by FWM or MI because both of them must generate symmetrical sidebands. Therefore, the newly created frequency components are probably caused by SRS. In fact, if

the Raman term is taken out of Eq. (1), the newly created frequency components truly disappear, as shown in the spectrogram displayed in Fig. 4. A further evidence showing that the newly created frequency components are caused by SRS will be given in the coherence analysis below.

Figure 5 shows the coherence and the spectrum of the generated SC at different propagation distances in the PCF for the same input pump pulse in Fig. 3. At the propagation distance of 30 cm, as shown in Fig. 5(a), the generated SC possesses a coherence degree of nearly 1 in the spectral range between 600 nm and 1900 nm except for a very small defect at 700 nm and a low-coherence gap near 1410 nm. It is not surprising that excellent coherence could be achieved outside the generated main SC (from 700 to 1410 nm) if one examines the SC spectrum shown in the figure, where the frequency products of OWB and FWM are extended far away from both sides of the main SC though they have very low spectral densities. In addition, the very small defect at 700 nm and the low-coherence gap near 1410 nm respectively correspond to the dips of the two sidebands (near 700 nm and 1410 nm) caused by OWB and FWM described above. Since the coherent spectral densities in such dips are relatively low initially, their SNRs are greatly degraded when the spontaneous Raman scattering and the input background noise are added to them, and thus get worsen inevitably as the Raman gain increases with the increase of the propagation distance. As a result, the small defect at 700 nm and the low-coherence gap near 1410 nm are formed, as displayed in Fig. 5(a).

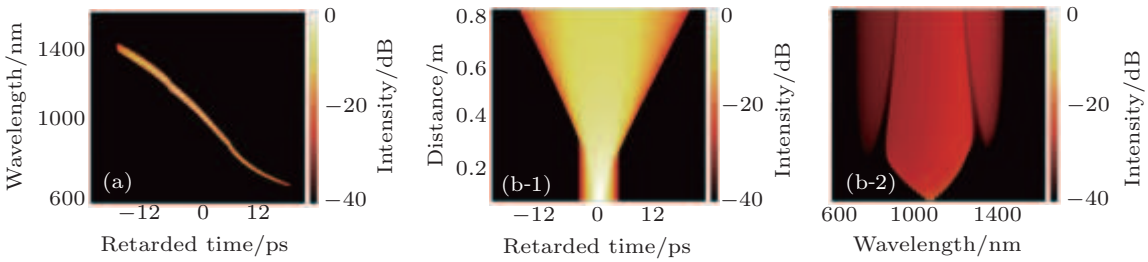


Fig. 4. (color online) (a) Time-frequency distributions at 80 cm in PCF and (b) pulse evolutions along PCF for the same pump pulse in Fig. 3 when the Raman term is taken out of the scalar GNLSE. All the figures are normalized by the corresponding maximum values.

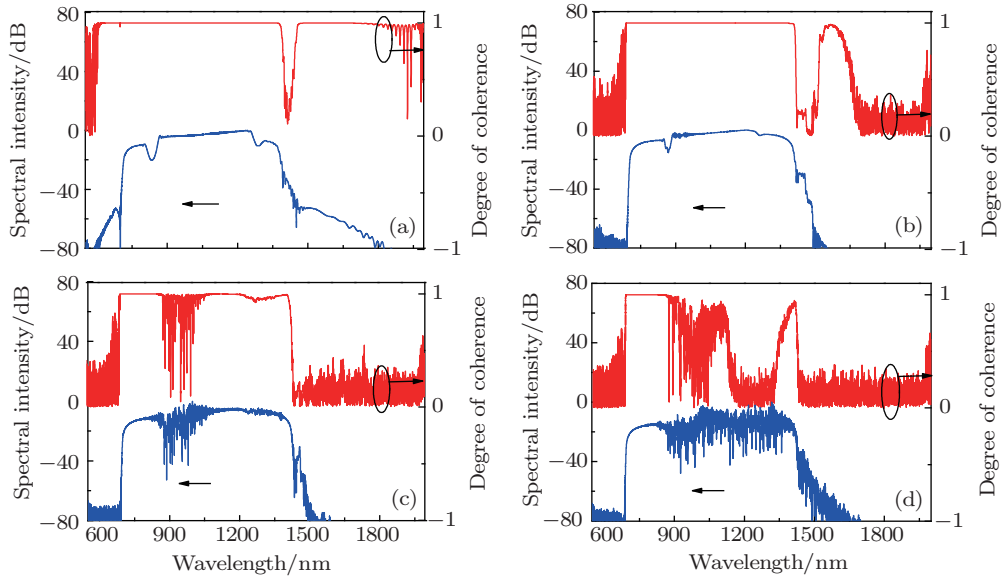


Fig. 5. (color online) Coherence and output spectrum of the generated SC for the same input pump pulse in Fig. 3 at the propagation distances of (a) 30 cm, (b) 50 cm, (c) 80 cm, and (d) 100 cm.

At the propagation distance of 50 cm, the spectral range with a coherence degree of nearly 1 is narrowed down to the main SC from 700 nm to 1410nm, as seen in Fig. 5(b). The coherence degrees in the short-wavelength region located on the left of the small defect at 700 nm (see Fig. 5(a)) are degraded from nearly 1 to very low values, probably because the coherent components in this region have Raman-shifted to longer wavelengths. Meanwhile, the coherence in the spectral range on the right of the low-coherence gap near 1410 nm is also degraded seriously, and a relatively high coherence can still be kept only in the narrow spectral range between 1520 nm and 1630 nm. This is because the low original SNR of the frequency components in this spectral range consequently gives rise to worse coherence degree when they are amplified by the

Raman gain and take part in the Raman frequency shift process continuously. Comparing Fig. 5(b) to Fig. 5(a), we note that the width of the low-coherence gap near 1410 nm becomes wider while a small peak grows up at 1430 nm in the spectrum, which further verify that the coherence degradation in this spectral range is caused by the Raman amplification for the low original SNR frequency components. As the noise accumulates with the propagation distance, at 80 cm where the noise has clearly been seen in the SC spectrum (Fig. 5(c)), only the main SC from 700 nm to 1410 nm can still maintain a relatively high coherence. However, the coherence is deteriorated near 900 nm, because the spectral position near 920 nm is very close to the gap at 820 nm formed by the short wavelength sideband generated by OWB and the broadened pulse spectrum (see Fig. 3(b)), and the initial SNR of the frequency components in this gap near 820 nm is also relatively low, with the combined effects of Raman amplification and Raman frequency-shift, the spectral positions with the low coherence degree are gradually moved to near 920 nm. For the similar reason, the coherence in the main SC from 700 nm to 1410 nm is further deteriorated to be very low, though the SC spectrum can still be distinguished when the propagation distance is 100 cm, as shown in Fig. 5(d). Therefore, it is very important for achieving high coherence across the generated SC to choose a suitable length of the ANDi PCF. According to the results shown in Fig. 5, for example, a high coherence across the generated SC may be achieved when the length of the ANDi PCF is designed to be 50 cm.

4. Conclusion

We have numerically investigated the SC generation in the ANDi PCF pumped with picosecond pulses by solving the scalar GNLSE. Our simulation results have shown that an octave SC with high power spectral density can be equally achieved by pumping the ANDi PCF with picosecond pulses. However, the PCF length required for the octave SC generation may have to be lengthened to several tens of centimeters, because the picosecond pulse has a narrower spectrum and thus has to propagate a long distance in the PCF to broaden its spectrum wide enough to make OWB and FWM take place. The relatively long PCF gives high Raman gain and strong Raman frequency shift, which degrades the coherence, in particular for the frequency components that have low spectral densities after OWB and FWM. Even so, an acceptable coherence can still be obtained across the generated SC by suitably choosing the length of the ANDi PCF.

References

[1] Udem T, Holzwarth R and Hänsch T W 2002 *Nature* **416** 233
[2] Povazay B, Bizheva K, Unterhuber A, Hermann B, Sattmann H, Fercher A F, DrexlerW, Apolonski A, WadsworthWJ, Knight J C, Russell P S, Vetterlein M and Scherzer E 2002 *Opt. Lett.* **27** 1800
[3] Paulsen H N, Hilligse K M, Thøgersen J, Keiding S R and Larsen J J 2003 *Opt. Lett.* **28** 1123
[4] Rinia H A, Bonn M, Müller M and Vartiainen E M 2007 *Chem. Phys. Chem.* **8** 279
[5] Schenkel B, Paschotta R and Keller U 2005 *J. Opt. Soc. Am. B* **22** 687
[6] Agrawal G P 2011 *J. Opt. Soc. Am. B* **28** A1
[7] Duan L N, Xueming L, Wang L R, Mao D and Wang G X 2011 *Laser Phys.* **21** 1813
[8] Lu H, Liu X M, Gong Y K, Hu X H and Li X H 2010 *J. Opt. Soc. Am. B* **27** 904
[9] Reeves W H, Skryabin D V, Biancalana F, Knight J C, Russell P St J, Omenetto F G, Efimov A and Taylor A J 2003 *Nature* **424** 511
[10] Dudley J M and Taylor J R 2009 *Nature Photon.* **3** 85
[11] Ranka J K, Windeler R S and Stentz A J 2000 *Opt. Lett.* **25** 25
[12] Rulkov A B, Vyatkin M Y, Popov S V, Taylor J R and Gapontsev V P 2005 *Opt. Express* **13** 377
[13] Yuan J H, Sang X Z, Yu C X, Xin X J, Shen X W, Zhang J L, Zhou G Y, Li S G and Hou L T 2011 *Chin. Phys. B* **20** 054210
[14] Dudley J M and Coen S 2006 *Rev. Mod. Phys.* **78** 1135
[15] Agrawal G P 2007 *Nonlinear Fiber Optics* (4rd edn.) (New York: Academic)
[16] Gu X, Kimmel M, Shreenath A, Trebino R, Dudley J M, Coen S and Windeler R 2003 *Opt. Express* **11** 2697
[17] Genty G, Coen S and Dudley J M 2007 *Opt. Soc. Am. B* **24** 1771
[18] Heidt A M 2010 *J. Opt. Soc. Am. B* **27** 550
[19] Heidt A M, Hartung A, Bosman G W, Krok P, Rohwer E G, Schwoerer H and Bartelt H 2011 *Opt. Express* **19** 3775
[20] Hooper L E, Mosley P J, Muir A C, Wadsworth W J and Knight J C 2011 *Opt. Express* **19** 4902
[21] Stolen R H, Gordon J P, Tomlinson W J and Haus H A 1989 *J. Opt. Soc. Am. B* **6** 1159
[22] Xueming L and Byoungho L 2003 *IEEE Photonic Tech. Lett.* **15** 1549
[23] Hult J 2008 *J. Lightwave Technol.* **25** 3770
[24] Dudley J M and Taylor J R 2010 *Supercontinuum Generation in Optical Fibers* (Cambridge: Cambridge University Press)
[25] Tu H, Liu Y, Lægsgaard J, Sharma U, Siegel M, Kopf D and Boppart S A 2010 *Opt. Express* **18** 27872
[26] Anderson D, Desaix M, Lisak M and Quiroga-Teixeiro M L 1992 *J. Opt. Soc. Am. B* **9** 1358
[27] Finot C, Kibler B, Provost L and Wabnitz S 2008 *J. Opt. Soc. Am. B* **25** 1938
[28] Fang X H, Hu M L, Chen X, Song Y J, Chai L and Wang C Y 2011 *Opt. Lett.* **36** 1005
[29] Song Y J, Hu M L, Xie C, Chai L and Wang Q Y 2010 *Acta Phys. Sin.* **59** 7105 (in Chinese)